Journal of Controlled Release 377 (2025) 162–173

Contents lists available at ScienceDirect

Journal of Controlled Release

journal homepage: www.elsevier.com/locate/jconrel

Exploring the impact of commonly used ionizable and pegylated lipids on mRNA-LNPs: A combined *in vitro* and preclinical perspective

Burcu Binici [a], Zahra Rattray [a], Assaf Zinger [b,c,d], Yvonne Perrie [a,*]

[a] Strathclyde Institute of Pharmacy and Biomedical Sciences, 161 Cathedral St, University of Strathclyde, Glasgow G4 0RE, UK
[b] Laboratory for Bioinspired Nano Engineering and Translational Therapeutics, Department of Chemical Engineering, Technion–Israel Institute of Technology, Haifa 3200003, Israel
[c] Cardiovascular Sciences Department, Houston Methodist Academic Institute, Houston, TX 77030, United States
[d] Neurosurgery Department, Houston Methodist Academic Institute, Houston, TX 77030, United States

ARTICLE INFO

Keywords:
mRNA
Lipid nanoparticles
Lipid composition
PEG lipids
Ionizable lipids
Potency
Efficacy

ABSTRACT

Ionizable lipids are widely recognized as the crucial component of lipid nanoparticles (LNPs). They enable mRNA encapsulation, shield it from enzymatic degradation, facilitate cellular uptake, and foster its cytosolic release for subsequent translation into proteins. In addition, PEGylated lipids are added to stabilize the particles in storage and *in vivo*. In this study, we investigate the potency of LNPs prepared using commonly adopted ionizable and pegylated lipids *in vitro* (using HEK293 cells) and *in vivo* (mouse studies) to consider the impact of structure on potency. LNPs were prepared using a fixed molar ratio of DSPC: Cholesterol: ionizable/cationic lipid: PEG lipid (10:38.5:50:1.5 mol%). All LNP formulations exhibited similar critical quality attributes (CQAs), including particle size <100 nm, low PDI (<0.2), near-neutral zeta potential, and high encapsulation efficiency (>90%). However, the potency of these LNPs, as measured by *in vitro* mRNA expression and *in vivo* expression following intramuscular injection in mice varied significantly. LNPs formulated with SM-102 exhibited the highest expression *in vitro*, whilst *in vivo* SM-102 and ALC-0315 LNPs showed significantly higher mRNA expression than DLin-MC3-DMA (MC3), DODAP and DOTAP LNPs. We also investigated the effect of PEG lipid choice (ALC-0159, DMG-PEG2k, and DSPE-PEG2k), which did not impact LNP CQAs, nor their clearance from the injection site. However, PEG lipid choice significantly influenced mRNA expression with the incorporation of DSPE-PEG2k reducing expression. This work contributes valuable insights to the evolving landscape of mRNA research, emphasizing that CQAs are a marker of the quality of the LNP production process, but not discriminatory regarding LNP potency. Similarly, standard *in vitro* studies do not provide insights into *in vivo* potency. These results further emphasize the intricacies of formulation design and the importance of bridging gaps between experimental outcomes in different settings.

1. Introduction

The recent development of messenger RNA (mRNA)-based vaccines has presented a highly encouraging approach to the rapid development of vaccines. The success of mRNA vaccines relies on using lipid nanoparticles (LNPs) by encapsulating mRNA in a lipid shell. Naked mRNA is a polyanionic macromolecule rapidly degraded by extracellular RNases, and cannot traverse cell membranes due to electrostatic repulsion. The encapsulation of mRNA into lipid vesicles enhances mRNA stability, facilitates cellular entry *via* endocytosis and improves expression compared to naked mRNA [1]. Moreover, LNPs have the potential to act as an adjuvant by augmenting the immune response [2]. Indeed, whilst LNP-induced inflammation present a challenge for therapeutic indications, this can be exploited for vaccine formulation [3]. It has been shown that the inflammatory response from mRNA-LNPs provides a basis for adjuvant activity, and ionizable lipids are likely responsible for

* Corresponding author at: Strathclyde Institute of Pharmacy and Biomedical Sciences, 161 Cathedral St, University of Strathclyde, Glasgow G4 0RE, UK.
E-mail address: yvonne.perrie@strath.ac.uk (Y. Perrie).

https://doi.org/10.1016/j.jconrel.2024.11.010
Received 5 August 2024; Received in revised form 27 October 2024; Accepted 5 November 2024

this due to their amine headgroups mediating pro-inflammatory cytokine release by activating pattern recognition receptors on the cell membrane [4]. Furthermore, results suggest that this adjuvant effect is influenced by the administration route of the LNPs [5].

LNPs are typically composed of four key types of lipids: an ionizable lipid, a PEGylated lipid, a phospholipid (often referred to as a helper lipid), and cholesterol. Helper lipids facilitate vesicle formation whilst reducing the ionizable lipid concentration to a level that allows for effective mRNA encapsulation [6]. Distearoylphosphatidylcholine (DSPC) is a commonly used phospholipid in nucleotide delivery; it enhances LNP stability due to its saturated carbon tail and high melting point. Dioleoylphosphatidylethanolamine (DOPE) is another phospholipid considered for the formulation of LNPs. It has a double bond in the acyl chains, making for a bulky tail and smaller head group compared to DSPC, creating a cone-shaped structure [7,8]. This structural feature improves intracellular nucleotide delivery by promoting the Hii phase but can also decrease LNP stability. Cholesterol is also commonly used in LNPs for particle formation and stability, bridging the gap between lipids in the LNP structure and facilitating endosomal release [9]. Currently, all approved mRNA-LNP products contain DSPC and cholesterol, albeit with differing ionizable and PEG lipids [10].

Early nucleic acid delivery systems relied on permanently cationic-charged lipids, but their use was limited by cytotoxicity concerns, mainly as they activate several cellular pathways, such as pro-apoptotic and pro-inflammatory cascades [11]. This led to the development of ionizable lipids, which switch from a positive charge in acidic pH (favouring their interaction with negatively charged mRNA) to neutral in physiological pH. Therefore, LNPs are formed at an acidic pH and then subjected to buffer exchange to achieve a pH of 7.4. Upon administration, LNPs are endocytosed, and the tertiary amine of the ionizable lipids is protonated to form a quaternary ammonium ion in the acidic environment of the endosome (pH ~4). Protonated ionizable lipids interact with anionic lipids of the endosome membrane, and this electrostatic interaction disrupts the endosomal membrane, releasing mRNA into the cytosol. The effectiveness of ionizable lipids is often linked to their pKa and 3D structural properties (Fig. 1). The pKa of LNPs should be sufficiently high to achieve protonation in acidic environments and sufficiently low to carry a smaller positive surface charge at physiological pH, minimizing toxicity [12]. The optimal pKa range of ionizable lipids to elicit an adaptive immune response *via* the intramuscular route has been reported as 6.6–6.9; however, this decreased to 6.2–6.6 for optimum protein expression following intravenous injection [13]. Another critical factor dictating lipid efficacy in LNPs is the molecular shape of ionizable lipids. Including branched tails within the ionizable lipid structure may lead to a cone-shaped geometry, thereby promoting endosomal escape [14].

Inclusion of PEGylated lipids within the LNP formulations offers steric stability to LNPs, which is crucial for particle integrity. Typically, 1.5 mol% of PEG lipid is used in clinically approved LNPs [15–17]. The PEG lipid content can affect LNP characteristics, such as the number of mRNA copies per LNP [18]. The length of the lipid tail of the PEG lipid also dictates the expression profile by affecting the desorption rate of the PEG chain [19,20]. After LNPs enter the body, it is proposed that the PEG chain needs to be released (*via* desorption) from the LNPs so that the LNPs can be internalized into the cells. The number and length of hydrophobic chains in the molecule drive the desorption rate of the PEG chains, and shorter PEG lipids such as DMG-PEG2k are commonly used [20]. Given the impact of these changes in formulation and the link to LNP function, our study aimed to investigate how the choice of commonly adopted ionizable and PEGylated lipids alters LNP physicochemical characteristics, *in vitro* efficacy and *in vivo* potency.

2. Materials and methods

2.1. Materials

1,2-distearoyl-sn-glycero-3-phosphocholine (DSPC), 1,2-dioleoyl-3-trimethylammoniumpropane (chloride salt) (DOTAP), 1,2-distearoyl-

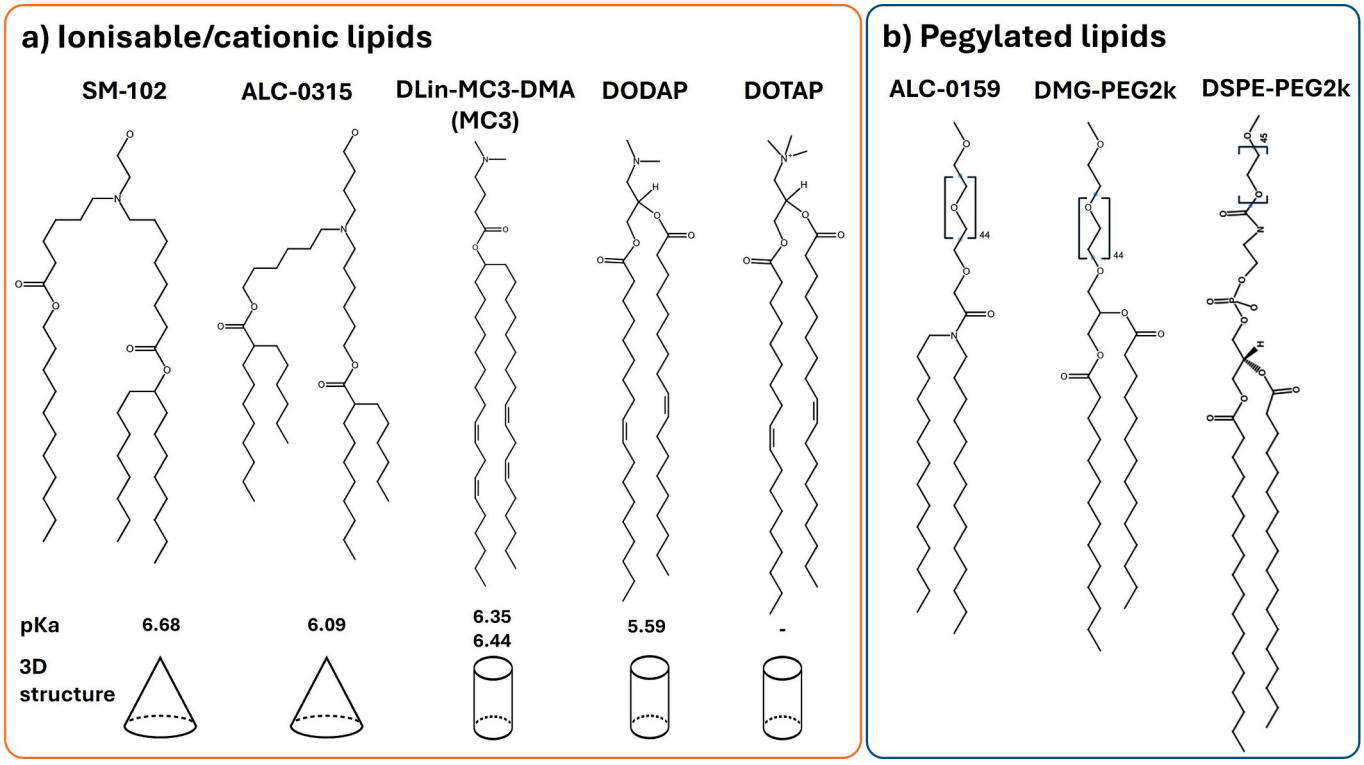

Fig. 1. The structures of the a) ionizable & cationic lipids and b) pegylated lipids used within this study. The structures were drawn using (Reaxys). The pKa for SM-102, ALC-0315 and MC3 are from [10] and for DODAP [21].

sn-glycero-3-phosphoethanolamine-N-[carbonyl-methoxy(polyethylene glycol)-2000] (sodium salt) (DSPE-PEG(2000)), 1,2-dimyristoyl-rac-glycero-3-methoxypolyethylene glycol-2000 (DMG-PEG2000), (1,2-dioleoyl-3-dimethylammonium propane) (DODAP), Polyadenylic acid (PolyA), Sodium citrate dihydrate, citric acid, Amicon® 10 kDa Ultra 15 mL Centrifugal Filters, dialysis membrane MWCO 12,000–14,000 Da, Cholesterol, Methoxypolyethyleneglycoloxy(2000)-N,N-ditetradecyla cetamide (ALC-0159) were purchased from Merck (Gillingham, UK). 8-[(2-hydroxyethyl)[6-oxo-6-(undecyloxy)hexyl]amino]-octanoic acid, 1-octylnonyl ester (SM-102) was purchased from ABP Biosciences (Maryland, USA). 4 Hydroxybutyl)azanediyl)bis(hexane-6,1-diyl)bis(2-hexyldecanoate (ALC-0315) was purchased from MedChem Express (MedChemtronica AB, Sollentuna, Sweden). O-(Z,Z,Z,*Z*-heptatriaconta-6,9,26,29-tetraen-19-yl)-4-(*N*,*N*-dimethylamino) (DLin-MC3-DMA (MC3)) was bought from Biorbyt (Cambridge, UK). EZ Cap™ Firefly Luciferase mRNA was obtained from APExBIO Technology (Stratech Scientific Ltd., Cambridge, UK). Minimum Essential Medium (MEM), Sodium Pyruvate (100 mM), UltraPure™ DNase/RNase-Free Distilled Water were purchased from Gibco™ (Paisley, UK). ONE-Glo™ Luciferase Assay System and VivoGlo luciferin were purchased from Promega (Southampton, UK). DiIC18(7) (1,1'-Dioctadecyl-3,3,3′,3'-Tetramethylindotricarbocyanine Iodide (DiR), Quant-it™ RiboGreen RNA Assay Kit, TrypLE™ Express Enzyme (1×), PBS - Phosphate-Buffered Saline (10×) pH 7.4 RNase-free were bought from ThermoFisher Scientific (Paisley, UK). BD Medical™ BD Micro-Fine™ Insulin Syringe was bought from Fisher Scientific (Loughborough, UK).

2.2. Preparation of lipid nanoparticles

Lipid nanoparticles (LNPs) were prepared using a staggered herringbone micromixer in the NanoAssemblr® Benchtop from Precision NanoSystems Inc. (Vancouver, BC, Canada). LNPs were prepared at an N/P ratio of 6 (the molar ratio of amine groups (N) of the ionizable lipid to that of phosphate groups (P) of mRNA). The lipid phase was composed of DSPC:Chol:cationic/ionizable: PEG lipid (10:38.5:50:1.5 mol%), and the aqueous phase was prepared with Fluc mRNA in citrate buffer pH 4. In the effect of ionizable lipid study, cationic LNPs were prepared with DOTAP and ionizable LNPs were prepared with ALC-0315, SM-102, MC3, or DODAP, whilst DMG-PEG2k was the PEGylated lipid (Table 1). When testing the PEG lipids, ALC-0159, DMG-PEG2k or DSPE-PEG2k were used as PEGylated lipids combined with ALC-0315, SM-102 or MC3 (Table 1). Lipids were dissolved in ethanol and mixed to the desired lipid ratio concentration. In the *in vivo* expression studies, DiR (1% molar of total lipid content), a lipophilic dye, was included in the lipid phase to track retention at the injection site, using a DIR filter at an excitation level spectrum of 754 nm and emission spectrum of 778 nm. Fluc mRNA was dissolved in 50 mM citrate buffer (pH 4) and 100 mM citrate buffer (pH 6) for ionizable LNPs and cationic LNPs (DOTAP), respectively. Lipids dissolved in ethanol and aqueous phase containing Fluc mRNA were injected simultaneously in the micromixer at a 3:1 aqueous:organic flow rate ratio (FRR) and a 12 mL/min total flow rate (TFR). Initial and final waste volumes were set at 0.15 and 0.05 mL, respectively.

2.3. Down-stream processing of LNPs

Dialysis (for cationic LNPs) or centrifugal filtration (for ionizable LNPs) was used to remove ethanol and adjust the formulation to pH 7.4. LNPs were dialyzed (MWCO 14 kDa) against PBS (pH 7.4) for one hour at ambient temperature under magnetic stirring. LNPs were diluted with PBS 40-fold and centrifuged (2000 ×*g* acceleration:9 deceleration:9) at 4 °C in the centrifugal filter unit (10 kDa MWCO) until re-concentrating LNPs to the required volume.

2.4. LNP characterization using dynamic light scattering

Following purification, particle size (z-average hydrodynamic diameter), polydispersity index (PDI) and zeta potential were measured by dynamic light scattering in Zetasizer Ultra (Malvern Panalytical Ltd., Worcestershire, UK), equipped with a 633 nm laser and a detection angle of 173°. Samples were diluted with PBS to a final lipid concentration of 0.1 mg/mL to measure particle size and polydispersity index (PDI). The same dilution with ultrapure water was used to measure zeta potential using electrophoretic mobility. Mean particle size, PDI, and zeta potential are expressed as the mean ± SD.

2.5. Entrapment efficiency and mRNA concentration within LNP formulations

The encapsulation efficiency (EE%) and mass balance (MB%) of LNPs were determined using the Quant-iT™ RiboGreen® RNA quantification kit, referring to the percentage of the encapsulated mRNA in the LNPs and total mRNA in the LNPs sample, respectively. 50 μL of the diluted sample (3 μg/mL of total mRNA LNPs with TE buffer) was incubated at 37 °C for 15 min with TE and 2% Triton X-100 (extracting encapsulated mRNA by bursting LNPs) to measure the amount of unencapsulated and total mRNA, respectively. 100 μL of Ribogreen fluorescent dye at 200 × and 500 × dilutions were added to the wells prepared with and without Triton X (only TE buffer), respectively. Fluorescence intensities were measured at excitation and emission wavelengths of 480 nm/520 nm using the GloMax® Discover Microplate Reader. EE% and mass balance% were calculated according to the standard curves prepared with naked mRNA in the absence and presence of Triton X.

2.6. In vitro cell viability and mRNA expression studies

HEK293 cells were cultivated in Minimum Essential Medium (MEM, Gibco) supplemented with 10% FBS, 1 mM sodium pyruvate, 50 U/mL penicillin-streptomycin at 37 °C in an environment containing 5% CO_2. HEK293 cells were sub-cultured at a density of 10,000 cells/well and incubated for 48 h at 37 °C, 5% CO_2. For all *in vitro* studies, mRNA-LNPs were diluted with cell growth media to 1, 0.5 or 0.25 μg/mL (100, 50 or 25 ng mRNA /100 μL). To measure cell viability, 100 μL of each LNP formulation was added to the wells (quadruplicate) and incubated for 24 h at 37 °C. The following day, 10 μL of Alamar blue was added to each well. Then, the plate was incubated for 4 h, and the fluorescence

Table 1
Corresponding mRNA-LNP compositions used in this study, equivalent to 5 μg Fluc mRNA/50 μL.

LNPs	DSPC (μg)	CHOL (μg)	Ionizable Lipids (μg)	PEG lipid (μg)	mRNA (μg)
ALC-0315	13.9	26.3	67.6	6.5	5
SM-102	13.9	26.3	62.7	6.6	5
MC3	13.9	26.2	56.7	6.6	5
DODAP	13.9	26.3	57.2	6.6	5
DOTAP	14.0	26.3	61.6	6.7	5

intensity was measured (λem = 530–560 nm, λex = 590 nm) using a fluorimeter (Polarstar Omega, BMG Labtech). To measure mRNA expression, HEK293 cells were treated with a serial dilution of mRNA-LNPs, as mentioned above. After 24 h of incubation, One-Glo substrate (100 μL) was added, and luciferase expression was detected using a plate reader (Polarstar Omega, BMG Labtech) as luminescence.

2.7. In vivo LNP retention at the injection site and mRNA expression

All animals were handled in accordance with the UK Home Office Animals Scientific Procedures Act of 1986 (UK project license number PP1650440/ personal license number I52241434) and in accordance with an internal ethics board. Groups of female 8–10 week old BALB/c mice (n = 5) were supplied by the Biological Procedure Unit at the University of Strathclyde, Glasgow. Preclinical imaging was performed using an *in vivo* imaging system (IVIS Spectrum, Perkin Elmer) and Living Image software ® 4.7.3 was used for image capture and data analysis. Mice were injected with 5 μg of DiR-labelled Fluc mRNA LNPs per leg *via* intramuscular (IM) injection and 6 h later, they were anaesthetized with 3% isoflurane and maintained at an isoflurane level of 2% in the IVIS chamber. Mice were imaged using the DiR filter (excitation/emission: 754/778 nm) to examine the biodistribution profile of DiR-labelled mRNA-LNPs. All mice subsequently received an intraperitoneal (IP) injection of d-luciferin at 150 mg/kg. Following IP injection (20 min), bioluminescence imaging was performed in an open filter using auto-exposure settings. DiR intensity and bioluminescence were measured at 6 h, 24 h, 48 h and 192 h post-IM injection of LNPs. Images and data were exported using Living Image software ® 4.7.3. Average radiant efficiency and total flux were determined by region of interest tools for fluorescence and bioluminescence signals by normalizing according to the control mice. Average radiant efficiency and total flux were calculated for the fluorescence intensity and bioluminescence measurements and expressed mean ± SEM.

2.8. Statistical analysis

Data are represented as a mean ± SD (phyisco-chemical properties) or SEM (*in vitro* expression, cell toxicity, *in vivo* biodistribution and *in vivo* expression). Graphpad Prism was used to perform statistical analysis by performing ANOVA with post-hoc analysis wherever applicable. P-value <0.05 was considered statistically significant.

3. Results

3.1. The effect of ionizable lipids on LNP phyisco-chemical properties

LNPs were prepared by mixing the lipid composition of DSPC: Chol: ionizable/cationic lipids: DMG-PEG2k (10:38.5:50:1.5 mol%) with Fluc mRNA at NP6 (Table 1), using a staggered herringbone micromixer and followed by purification with PBS. All LNPs were < 100 nm in diameter, with low PDI (<0.2) and near neutral zeta potential (Table 2). Irrespective of the choice of ionizable (SM-102, ALC-0315, MC3 or DODAP) or cationic (DOTAP) lipid, mRNA encapsulation was >90%, and mRNA mass balance (total mRNA content) was high (>85%) (Table 2). The seven-day stability profile of these LNPs at storage temperature (2–8 °C) is shown in Table 2. LNPs prepared with ionizable lipids showed a stable profile, while the size of DOTAP-LNPs increased by approximately 15 nm (Table 2). The zeta potential of LNPs did not change significantly, nor did the encapsulation efficiency and mRNA mass balance (which remained >90% and 85%, respectively, for all formulations; Table 2), confirming their short-term stability and suitability for *in vitro* and *in vivo* studies.

3.2. The effect of ionisable lipid composition on in vitro mRNA-LNP expression

To investigate *in vitro* efficacy, HEK293 cells were treated with Fluc-mRNA-LNPs for 24 h. Subsequently, cell viability and mRNA (luciferase) expression were also measured (Fig. 2). Across all test concentrations, no notable impact on cell viability was observed (Fig. 2a–e). Regarding mRNA expression (Fig. 2f–j), expression levels were variable, with SM-102 levels approx. 13-fold higher than MC3-LNPs, and approx. 300-fold higher than ALC-0315. Notably, mRNA expression for DODAP and DOTAP was low (approx. 1500 and 500 fold lower than SM-102, respectively; Fig. 2f–j).

3.3. The effect of ionizable lipid composition on in vivo mRNA-LNP retention

To consider the *in vivo* expression and LNP retention at the injection site, BALB/c mice were intramuscularly injected in both hind legs with Fluc 5 μg mRNA formulated in the 5 different DiR-labelled LNPs (Fig. 3). DiR-labelling of the LNPs is a commonly adopted protocol to allow tracking of LNPs (*e.g.* [22–25]), and we used it to consider whether expression profiles at the injection site were linked to LNP clearance. The phyisco-chemical characteristics of the mRNA-LNPs with DiR are shown in Table S1. The results show that DiR-retention was only detected at the injection site, as detecting the fluorescence intensity in internal organs with IVIS without organ extraction is difficult due to limited penetration depth in tissue (Fig. 3a). Interestingly, whilst all mice received the same dose of DiR-labelled LNPs, after 6 h the fluorescent intensity at the injection site was higher for three out of the four ionizable LNPs (ALC-0315, SM-102 and MC3), whilst DODAP and DOTAP LNP DiR levels remained low (and remained low across the timescale of the study (Fig. 3b). After 6 h, SM-102 LNPs were cleared from the injection site more rapidly than LNPs containing either ALC-0315 or MC3 as the ionizable lipid (Figs. 3a and b). The difference in clearance rates from the injection site is exemplified in the AUC (Fig. 3c), with LNPs composed of ALC-0315 and MC3 having similar AUC and significantly higher (p < 0.05) than SM-102 LNPs. Similarly,

Table 2
The physicochemical properties of LNPs prepared with various ionizable/cationic lipids. LNPs comprised DSPC: Chol: ionizable/cationic lipid: DMG-PEG2k (10:38.5:50:1.5 M ratio) and encapsulated Fluc mRNA at NP6. Ionizable lipids are ALC-0315, SM-102, MC3 (DLin-MC3-DMA) and DODAP, while the cationic lipid is DOTAP. LNPs were stored in the fridge (2–8 °C). Characteristics were measured at 0 and 7 days. Results represent mean ± SD, n = 3 independent batches.

Cationic/Ionizable lipids	Day	Diameter (nm)	PDI	Zeta potential (mV)	EE (%)	Mass balance (%)
SM-102	0	64.9 ± 5.3	0.04 ± 0.03	−1.0 ± 0.9	97 ± 1	85 ± 16
	7	67.9 ± 6.8	0.03 ± 0.01	−1.5 ± 0.9	96 ± 0	84 ± 14
ALC-0315	0	55.2 ± 0.5	0.11 ± 0.02	−2.1 ± 1.1	93 ± 2	93 ± 11
	7	56.3 ± 1.0	0.12 ± 0.02	−3.7 ± 2.3	95 ± 1	100 ± 1
MC3	0	60.8 ± 1.3	0.11 ± 0.02	−1.6 ± 1.6	93 ± 2	93 ± 5
	7	60.6 ± 2.0	0.10 ± 0.02	−2.2 ± 0.5	93 ± 1	93 ± 6
DODAP	0	69.0 ± 2.8	0.04 ± 0.02	−1.4 ± 1.3	91 ± 1	97 ± 6
	7	66.1 ± 7.5	0.06 ± 0.02	−1.4 ± 1.0	87 ± 2	94 ± 2
DOTAP	0	49.8 ± 5.9	0.24 ± 0.04	2.4 ± 1.9	99 ± 0	89 ± 10
	7	68.7 ± 10.9	0.29 ± 0.03	4.8 ± 1.2	99 ± 1	87 ± 8

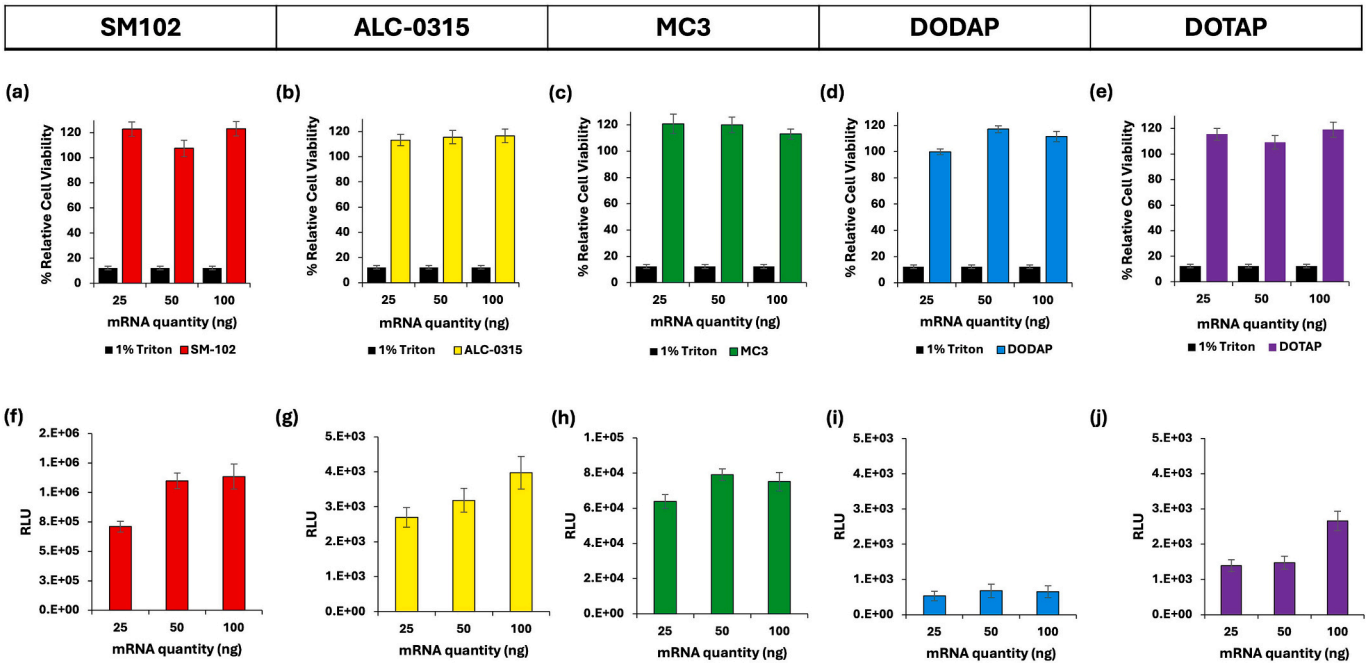

Fig. 2. Toxicity profile and *in vitro* transfection efficiency of Fluc mRNA LNPs. HEK293 cells were transfected with Fluc mRNA LNPs at mRNA of 25 ng, 50 ng, or 100 ng for all the formulations. 24-h post LNPs incubation a-e) HEK293 cell biocompatibility using Alamar blue, f-j) luminescence intensity was measured. LNPs comprised DSPC: Chol: ionizable/cationic lipid:DMG-PEG2k (10:38.5:50:1.5 M ratio) and encapsulated Fluc mRNA at NP6. Ionizable lipids are ALC-0315, SM-102, MC3, and DODAP, while cationic lipid is DOTAP. Results represent mean ± SEM ($n = 3$) of three independent experiments. (For interpretation of the references to colour in this figure legend, the reader is referred to the web version of this article.)

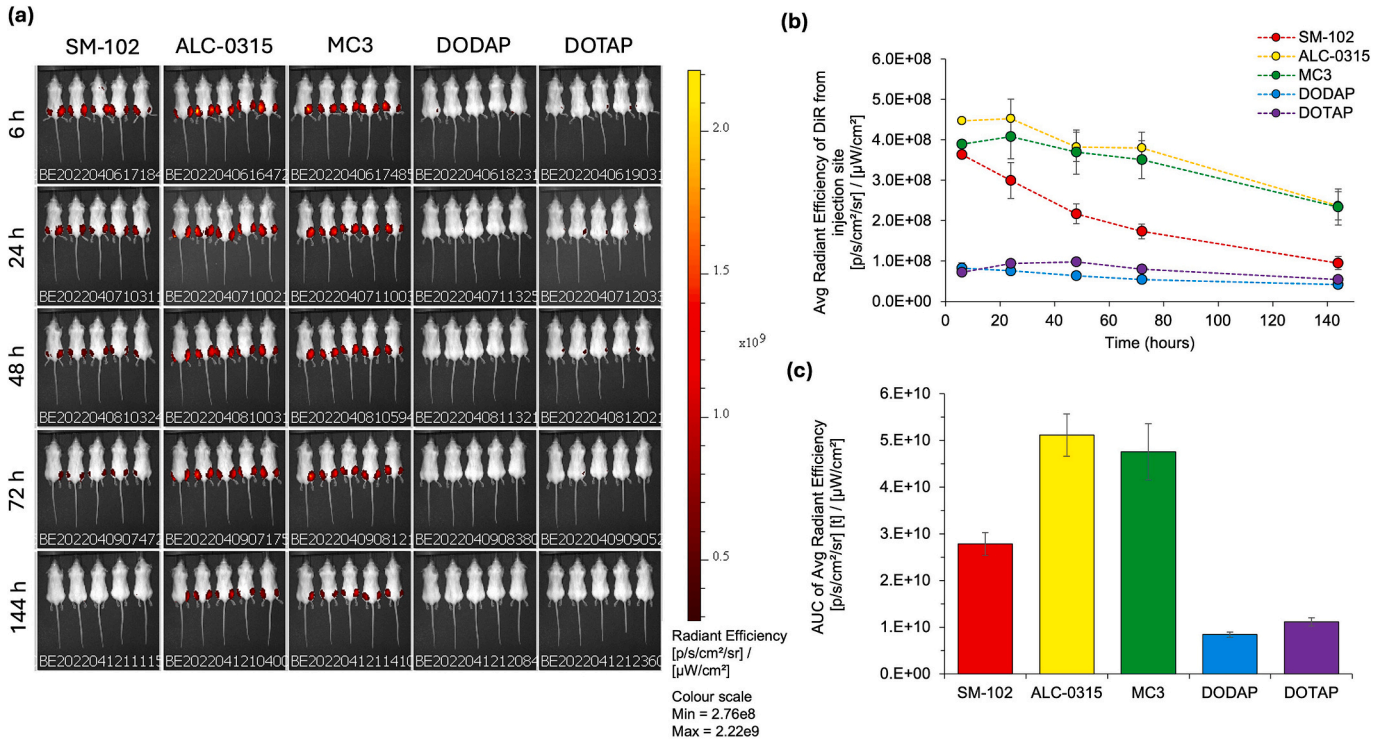

Fig. 3. LNP retention at the injection site. Female BALB/c mice were intramuscularly injected with DiR-labelled Fluc mRNA-LNPs, and the fluorescence intensity was measured at various time points (6–144 h). The injected mRNA dose was 5 µg mRNA encapsulated in LNPs composed of DSPC: Chol: ionizable/cationic lipids: DMG-PEG2k. The ionizable lipids are ALC-0315, SM-102, MC3, and DODAP, while the cationic lipid is DOTAP. a) Representative IVIS images at selected time points after DiR-labelled mRNA-LNP injection. b) Fluorescence signal at the injection site over 144 h and c) the Area Under the Curve (AUC). Results represent mean ± SEM (5 mice, 1 injection per hind leg; 10 data points). Connecting lines are for presentation purposes only.

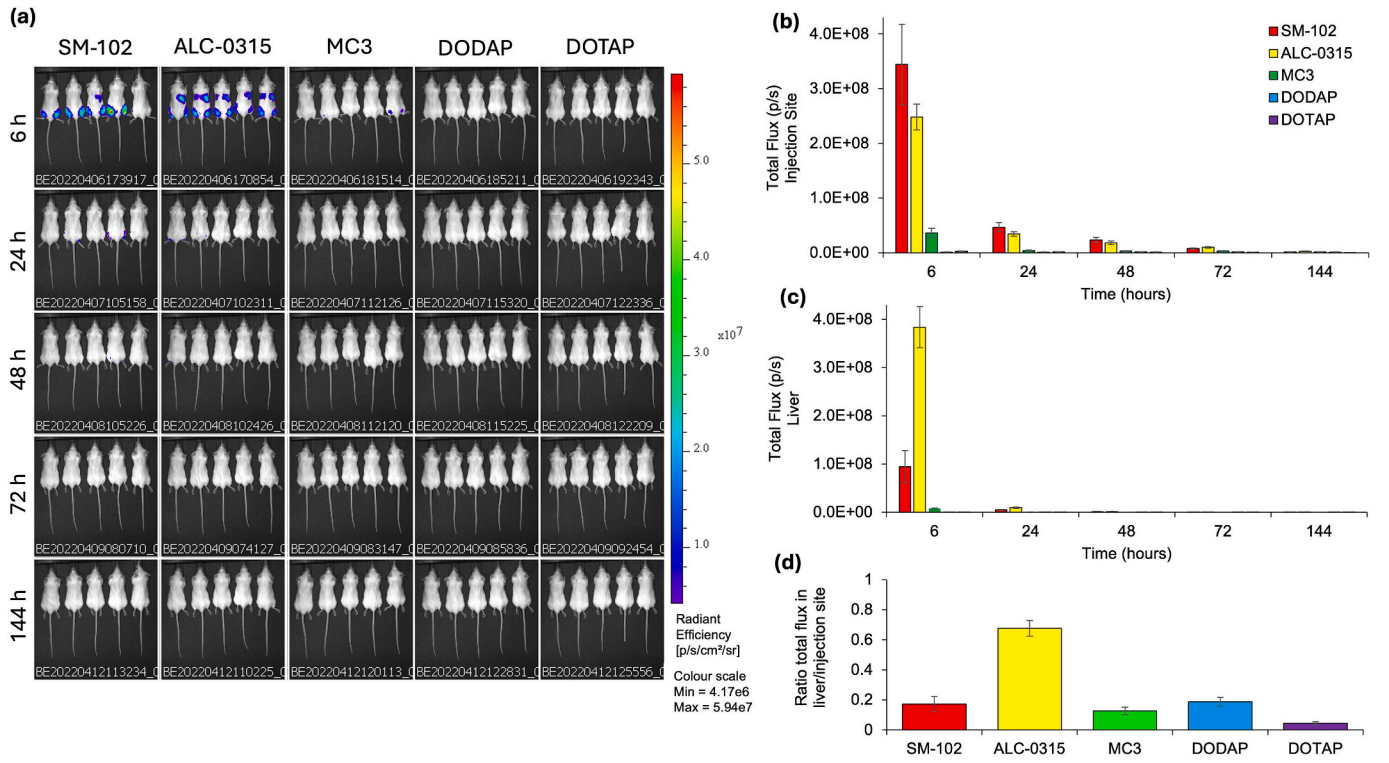

Fig. 4. Comparison of mRNA-encoded luciferase expression when formulated in different LNPs. The female BALB/c mice from Fig. 3 were also imaged for luciferase expression. Mice were intramuscularly injected with DiR-labelled mRNA-LNPs, and the flux was measured at various time points (6–144 h). The injected mRNA dose was 5 μg mRNA encapsulated in LNPs composed of DSPC: Chol: ionizable/cationic lipids: DMG-PEG2k. The ionizable lipids are ALC-0315, SM-102, MC3, and DODAP, while the cationic lipid is DOTAP. a) Representative IVIS images at selected time points b) Luminescence signal per injection site over 144 h, c) Luminescence signal per liver over 144 h, and d) ratio of total flux in liver/injection site (both legs). Results represent mean ± SEM (5 mice, 1 injection per hind leg; 10 data points).

DODAP and DOTAP LNPs have a significantly lower ($p < 0.05$) AUC than SM-102. These results suggest that the choice of ionizable/cationic lipids in LNPs rather than their CQAs affects their clearance rate from the injection site.

3.4. The effect of ionizable lipid composition on in vivo mRNA-LNP expression

The same mice were simultaneously analyzed for mRNA protein (luciferase) expression (Fig. 4). The results show distinct patterns over time and across different LNPs. At 6 h post-injection, the highest luciferase expression occurred at the injection site and liver (Fig. 4). The potency ranking for luciferase expression at the injection site for the LNPs was ALC-0315 ≈ SM-102 > > MC3 >> DOTAP ≥ DODAP (Fig. 4b). LNPs prepared using ALC-0315 and SM-102 showed comparable expression levels, with levels approximately 8-fold higher than MC3-LNPs and 180-fold higher compared to DODAP and DOTAP LNPs (which had similar levels of expression) (Fig. 4b). Luciferase expression can also be seen in the liver for SM-102 and ALC-0315 LNPs (Fig. 4c). When considering the balance between expression at the injection site and the liver, ALC-0315 LNPs demonstrated significantly ($p < 0.05$) higher liver expression than SM-102 LNPs (Fig. 4d). These findings further indicate that the selection of ionizable or cationic lipids in LNP formulations significantly influences the distribution of mRNA expression, even when all LNPs share comparable critical quality attributes (CQAs).

3.5. The impact of pegylated lipids on Fluc-mRNA LNP characteristics and potency

Given the effect of ionizable lipids *in vitro* and *in vivo*, we selected ALC-0315, SM-102 and MC3 as lead lipids and tested these lipids combined with three different PEG types used in the marketed products. These PEGylated lipids were ALC-0159, DMG-PEG2k and DSPE-PEG2k, which are used in Comirnaty®, Spikevax® and Doxil®, respectively. DSPC and cholesterol were included, as reported in Table 1. All LNPs had a diameter < 100 nm, a low PDI (<0.2), a neutral surface charge, and > 90% mRNA entrapment efficiency and mass balance. (Table 3).

ALC-0315 and SM-102 LNPs were then tested in HEK293 cells for their mRNA expression potency by measuring luciferase expression (Fig. 5). Again, we see the same trend with LNPs prepared with SM-102 promoting significantly higher ($p < 0.05$) expression than ALC-0315 LNPs when comparing between each of the PEG lipid coutnerparts (Fig. 5). However, we also demonstrate that using ALC-0159 PEG lipid significantly ($p < 0.05$) increased expression in comparison to DMG-PEG2k (Fig. 5). Indeed, using ALC-0159 instead of DMG-PEG2k at the same 1.5% ratio within the formulations enhanced the mRNA expression 9-fold and 4-fold for ALC-0315 and SM-102-based LNPs, respectively (Fig. 5).

3.6. The effect of PEGylated lipid choice on in vivo mRNA-LNP distribution and expression

To consider the impact of the choice of PEGylated lipid within the LNPs on the biodistribution and potency *in vivo*, BALB/c mice were injected with 5 μg of DiR-labelled LNPs encapsulated Fluc mRNA prepared with SM-102 (Fig. 6), ALC-0315 (Fig. 7) or MC3 (Fig. 8) as the ionizable lipid. Our results demonstrate that the choice of PEGylated lipid (DSPE-PEG2k *vs* DMG-PEG2k *vs* ALC-0159) has no notable impact on SM-102 LNP retention at the injection site (Figs. 6a and b) nor the calculated AUC (Fig. 6c). However, the choice of PEGylated lipid has a major impact on protein expression (Fig. 6d), with the use of DSPE-

Table 3
Physicochemical properties of LNPs prepared with different PEGylated lipids. The LNPs comprised DSPC: Chol: ionizable lipid: PEG lipid (10:38.5:50:1.5 M ratio) and encapsulated Fluc mRNA at NP6. Ionizable lipids are ALC-0315, SM-102 and MC3, while PEG lipids are ALC-0159, DMG-PEG2k and DSPE-PEG2k. They were manufactured using microfluidics at a 3:1 FRR and 12 mL/min TFR and purified by a spin column. After purification, average diameter, PDI and zeta potential were measured using DLS. Encapsulation efficiency and mass balance were measured using a Ribogreen kit.

Ionizable lipid	Pegylated lipid	Diameter (nm)	PDI	Zeta potential (mV)	EE (%)	Mass balance (%)
SM-102	ALC-0159	73.5 ± 2.5	0.05 ± 0.03	−1.7 ± 1.1	94 ± 3	91 ± 11
	DMG-PEG2k	66.4 ± 2.7	0.08 ± 0.01	−2.4 ± 0.7	91 ± 5	86 ± 12
	DSPE-PEG2k	63.4 ± 0.1	0.04 ± 0.02	−2.3 ± 2.2	97	92
ALC-0315	ALC-0159	74.5 ± 5.1	0.08 ± 0.03	−2.8 ± 1.1	92 ± 4	96 ± 8
	DMG-PEG2k	57.3 ± 3.0	0.11 ± 0.03	−3.0 ± 1.5	93 ± 2	92 ± 11
	DSPE-PEG2k	57.4 ± 0.4	0.04 ± 0.01	−2.5 ± 2.2	95	100
MC3	ALC-0159	77.0 ± 0.7	0.10 ± 0.07	−5.6 ± 0.5	99	98
	DMG-PEG2k	70.1 ± 0.3	0.09 ± 0.02	−11.1 ± 1.1	98	91
	DSPE-PEG2k	69.2 ± 0.6	0.07 ± 0.02	−6.3 ± 1.4	99	85

PEG2k within the LNPs significantly ($P < 0.05$) reducing expression compared to LNPs prepared with ALC-0159 or DMG-PEG2k (which are not significantly different) both at the injection site (Fig. 6e and f) and the liver (Fig. 6g and h). Therefore, the different expression levels measured at the injection site do not result from differences in clearance.

In the case of ALC-0315 LNPs (Fig. 7), the choice of pegylated lipid again had no impact on LNPs clearance (Fig. 7a) from the injection site, with similar LNP retention for ALC-0315 LNPs prepared with DSPE-PEG2k, DMG-PEG2k and ALC-0159 (Fig. 7b and c). Again similar to SM-102, Fluc protein expression was significantly ($p < 0.05$) lower for LNPs prepared with DSPE-PEG2k both at the injection site (Fig. 7d, e and f) and liver (Fig. 7d, g and h) compared to LNPs prepared with ALC-0159 and DMG-PEG2k. However, unlike the SM-102 LNPs, LNPs prepared with the ionizable lipid ALC-0315 in combination with the pegylated lipid ALC-0159 gave significantly ($p < 0.05$) higher expression both at the injection site (Fig. 7e and f) and the liver (Fig. 7g and h) than LNPs prepared with DMG-PEG2k.

When we combined MC3 ionizable lipid with these PEG lipids (Fig. 8), again we see a similar trend, with choice of PEG lipid having no significant impact on retention profile at the injection site (Fig. 8a and b) or the calculated AUC (Fig. 8c). Also again the mRNA Fluc expression is significantly lower for LNPs prepared with DSPE-PEG2k ($p < 0.05$) both at the injection site (Fig. 8d, e and f) and the liver (Fig. 8d, g and h) in comparison to LNPs PEGylated with ALC-0159 and DMG-PEG2k. Overall, from these results, we see that irrespective of the ionizable lipid used, using DSPE-PEG reduces the mRNA expression profile of the LNPs, and this is not linked to their clearance from the injection site.

4. Discussion

This study compared mRNA-LNPs formulated from five commonly used ionizable/cationic lipids and three PEGylated lipids to investigate how these lipids alter LNP physico-chemical characteristics, *in vitro* efficacy, *in vivo* expression, and retention at the injection site. All formulations had a fixed molar ratio of DSPC: Chol: Ionizable/cationic lipid: PEG lipid (10:38.5:50:1.5%).

The physico-chemical characteristics measured within our studies are often monitored as CQAs, and here we demonstrated that the choice of ionizable or cationic lipids (Table 2) had no notable impact on these CQAs. All LNPs prepared with the various ionizable lipids were consistently <100 nm in size, with a low polydispersity (<0.2 PDI), a near-neutral zeta potential, high (>90%) encapsulation efficiency and mass balance (Table 2). Despite these similarities in CQA, the LNPs showed different potencies in both *in vitro* and *in vivo* and potency *in vitro* and *in vivo* did not correlate (Figs. 2 to 4). This lack of *in vitro*-invivo correlation has also been noted in other studies [26–28] and suggests alternative cell lines should be explored.

The ionizable lipid is generally considered the most essential component in the LNPs, with the structure of the ionizable lipid influencing the expression profile of LNPs (*e.g.* [14,29]). Within our studies, SM-102 LNPs were the most effective *in vitro*, and the two most effective LNP formulations *in vivo* contained SM-102 and ALC-0315. These two lipids contain an amino-alcohol head group with pKas of 6.68 and 6.09, respectively (Fig. 1). It has been reported that the optimum pKa for an mRNA vaccine is 6.6–6.9 [13]. Whilst this link to pKa could be used to

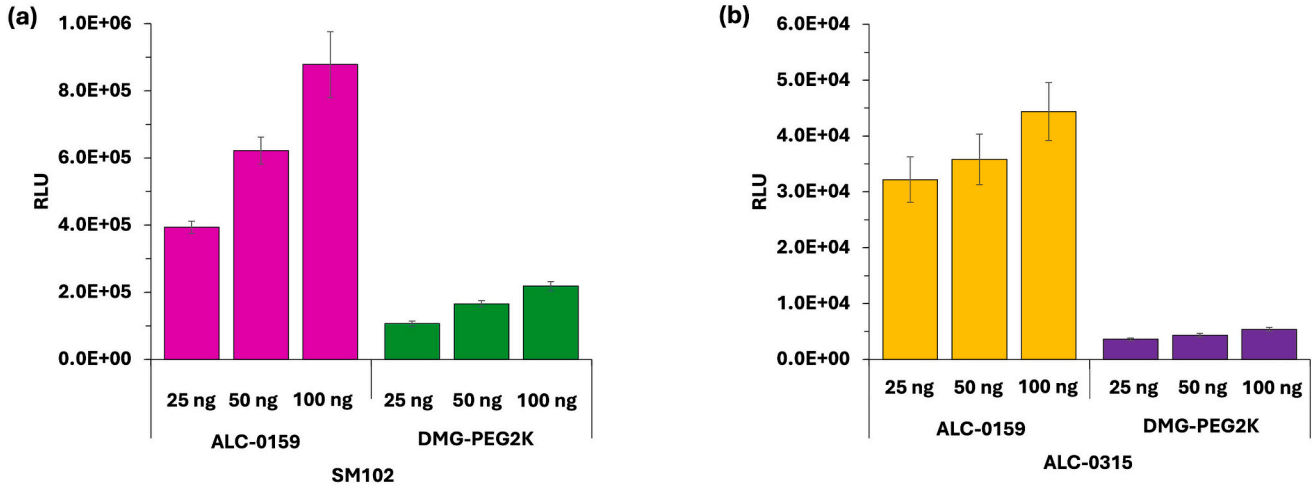

Fig. 5. The effect of PEGylated lipids on *in vitro* expression efficiency. HEK293 cells were transfected with Fluc mRNA LNPs at mRNA levels of 25 ng, 50 ng, and 100 ng for all the formulations. 24-h post LNPs incubation luminescence intensity was measured. The LNPs comprised DSPC: Chol: ionizable: PEG lipid (10:38.5:50:1.5 M ratio) and encapsulated Fluc mRNA at NP6. Ionizable lipids are a) SM-102 with ALC-0159 or DMG-PEG2k and b) ALC-0315 with ALC-0159 or DMG-PEG2k. Results represent mean ± SEM, $n = 3$ independent batches.

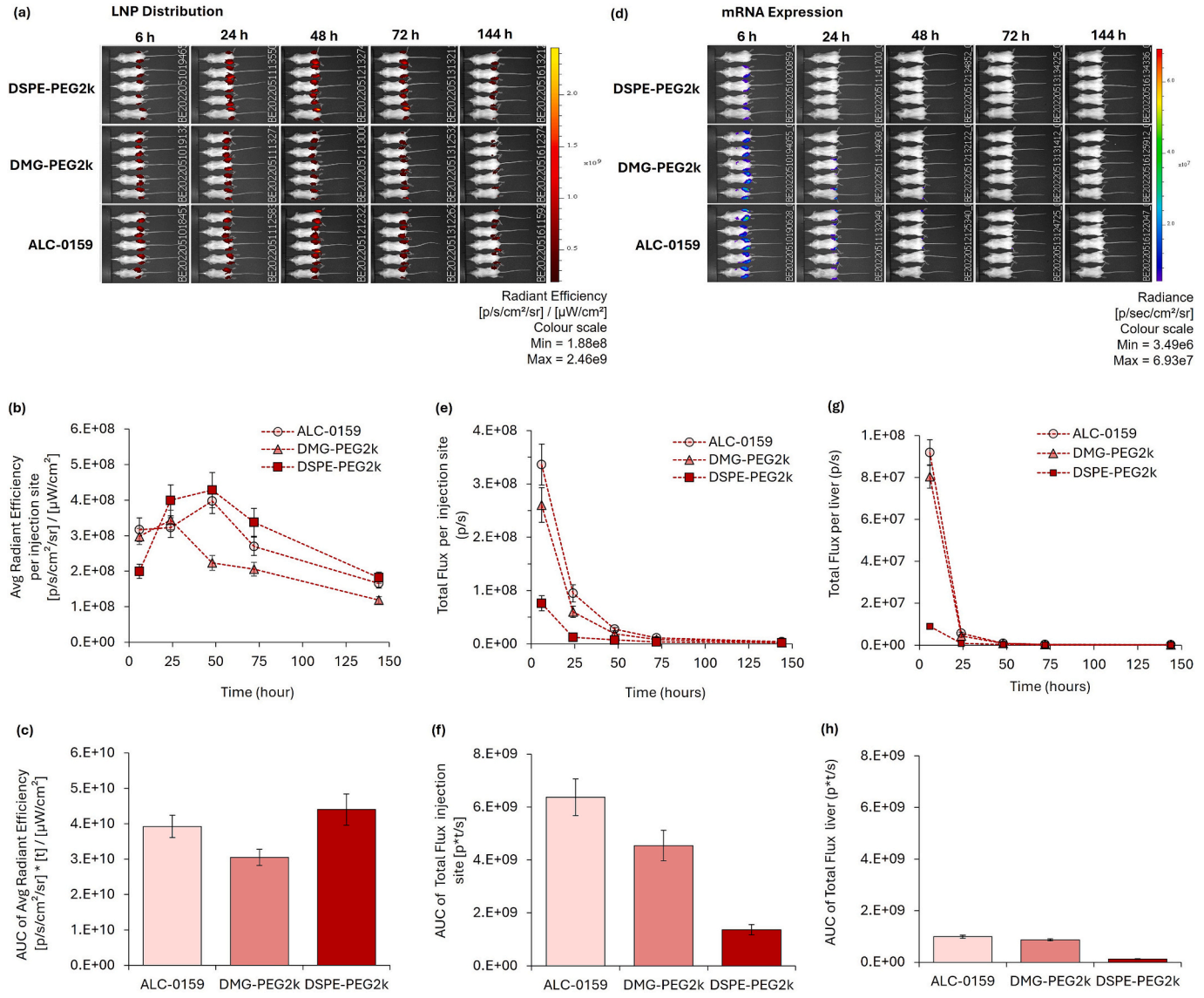

Fig. 6. Biodistribution and expression profile of SM-102 Fluc mRNA-LNPs labelled with DiR prepared with three different PEGylated lipids (ALC-0159, DMG-PEG2k and DSPE-PEG2k), a) IVIS image representing the biodistribution profile of DiR labelled LNPs and b) the quantification of DIR intensity from the injection site over the time and c) the Area Under the Curve (AUC). d) Representative IVIS image of the expression profile of the LNPs formulated with Fluc mRNA and quantification of the luminescence signal as the light emitted from e) the injection site and corresponding f) Area Under the Curve (AUC) g) liver and corresponding the Area Under the Curve (AUC). The LNPs comprised DSPC: Chol: SM-102: PEG lipid (10:38.5:50:1.5 M ratio) and encapsulated Fluc mRNA at NP6. PEG lipids are ALC-0159, DMG-PEG2k and DSPE-PEG2k. Female BALB/c mice were injected with 5 µg of Fluc mRNA-LNPs. Results represent mean ± SEM (5 mice, 1 injection per hind leg; 10 data points).

explain the lower expression from MC3-based LNPs, this conflicts with the high expression seen with *in vivo* ALC-0315 (which has a pKa of 6.09; Fig. 1). This suggests that the pKa of the ionizable lipid is not the only driving force for effective mRNA expression. When considering the molecular geometry, SM-102 and ALC-0315 have branched hydrocarbon lipid tails that may create a more cone-shaped structure than MC3, DODAP and DOTAP, and this has been reported to improve expression by enhancing endosomal release [14,30–33]. This supports the improved efficacy of SM-102 and ALC-0315 LNPs seen in our *in vivo* studies (Figs. 3 and 4). However it remains unclear why ALC-0315 LNPs do not perform well *in vitro*.

mRNA expression at both the injection site and the liver after intrasmuscular injection is seen in our studies here and elsewhere [34]. In both our studies, as well as in those of Mancino et al., protein expression was observed in the liver despite the absence of detectable fluorescence, which could stem from the localized uptake of LNPs into the bloodstream following intramuscular administration. Once in circulation, LNPs are rapidly transported to the liver (a pattern well-documented for IV administration), where they are taken up by hepatocytes, leading to protein translation [34]. The hepatic tropism of ALC-0315 LNPs compared with SM-102 LNPs after i.m. injection shown in our studies has also been demonstrated by Zhang *et al* investigating the expression kinetics of LNPs [28]. Similarly, it has been shown that ALC-0315 exhibits a higher expression profile in the liver compared to MC3, which is specifically designed to target hepatocytes for the knockdown of transthyretin [35]. Unlike MC3, both SM-102 and ALC-0315 contain biodegradable linkages, which are reported to improve their pharmacokinetics properties and reduce toxicities [36,37]. Differences in the ratio of expression between the injection site and the liver for LNPs and nanoparticles, in general, could be related to 1) LNP physico-chemical characteristics, which in turn affect clearance to the liver, 2) particle uptake and metabolism in the liver, and/or 3) immune responses

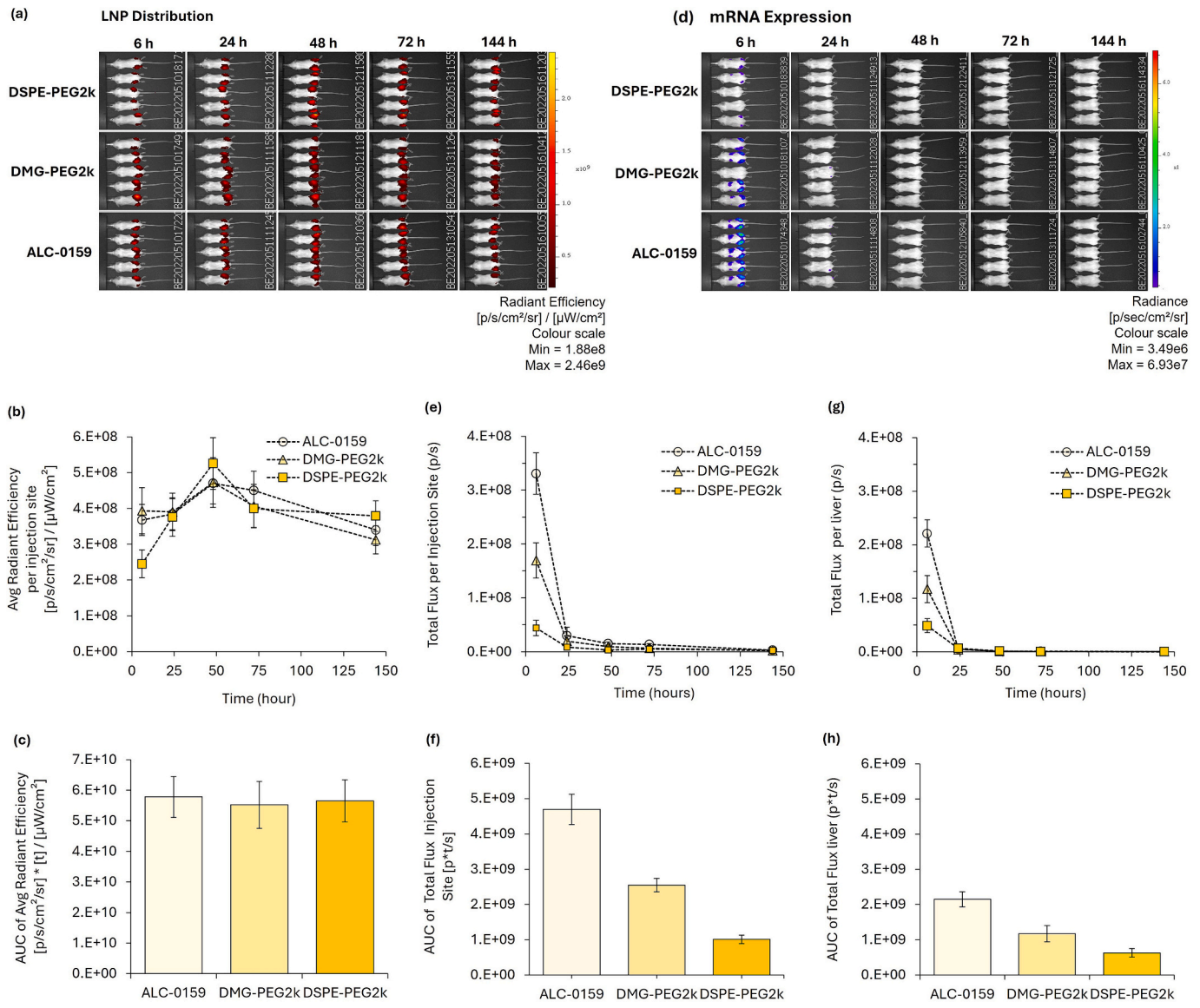

Fig. 7. Biodistribution and expression profile of ALC-0315 Fluc mRNA-LNPs labelled with DiR prepared with three different PEGylated lipids (ALC-0159, DMG-PEG2k and DSPE-PEG2k), a) IVIS image representing the biodistribution profile of DiR labelled LNPs and b) the quantification of DIR intensity from the injection site over the time and c) the Area Under the Curve (AUC). d) Representative IVIS image of the expression profile of the LNPs formulated with Fluc mRNAand quantification of the luminescence signal as the light emitted from e) the injection site and g) corresponding Area Under the Curve (AUC) g) liver and corresponding h) the Area Under the Curve (AUC). The LNPs comprised DSPC: Chol: ALC-0315: PEG lipid (10:38.5:50:1.5 M ratio) and encapsulated Fluc mRNA at NP6. PEG lipids are ALC-0159, DMG-PEG2k and DSPE-PEG2k. Female BALB/c mice were injected with 5 µg of Fluc mRNA-LNPs. Results represent mean ± SEM (5 mice, 1 injection per hind leg; 10 data points).

triggered by LNPs. Given the similarities in the LNP physico-chemical attributes (Table 2), this suggests that the physico-chemical attributes are not a key driving factor. Indeed, it has been shown that the design of the branched tails of ionizable lipids within the LNPs, and not the CQA of the LNPs, drives the distribution of LNPs [38]. This suggests differences in metabolism and/or immunogenicity of the ionizable lipids drive these differences and given that *in vitro* studies lacking metabolic and immune functionality, they do not adequately predict *in vivo* performance [27]. This highlights that the CQAs generally reported for LNPs are a good indicator of quality (and hence valuable critical quality attributes when considering manufacturing) but are not necessarily potency-indicating.

We further considered the impact of the choice of PEGylated lipid used within the formulation and selected SM-102, ALC-0315 and MC3 based LNPs. Again, physico-chemically, the particles were similar (Table 3), and SM-102 LNPs outperformed ALC-0315 LNPs in HEK293 cells, irrespective of the PEGylated lipid used (ALC-0159 *vs* DMG-PEG2k). However, with both ionizable lipids, using ALC-0159 in the LNP composition rather than DMG-PEG2k resulted in higher *in vitro* expression (Fig. 5). These LNPs were then tested *in vivo* and along with the addition of MC3 as a third ionizable lipid and DSPE-PEG2k as an additional PEG lipid. DSPE-PEG2k is used to sterically stabilize DOXIL liposomes *in vivo* and has an 18-carbon tail compared to ALC-0159 and DMG-PEG2k (which have 14 carbon tails). While the choice of PEG-lipid did not influence clearance from the injection site, luciferase expression was impacted, with the use of DSPE-PEG2k reducing the luciferase expression from SM-102 LNPs (Fig. 6), ALC-0315 LNPs (Fig. 7) and MC3 LNPs (Fig. 8).

PEGylated lipids are incorporated into LNP formulations to provide stability through steric stabilization both in the vial and within the biological milieu. The length of the lipid tail of these PEGylated lipids plays a crucial role in determining the fate of LNPs *in vivo*. Specifically, C18 acyl chains exhibit efficient anchoring in the membrane. On the

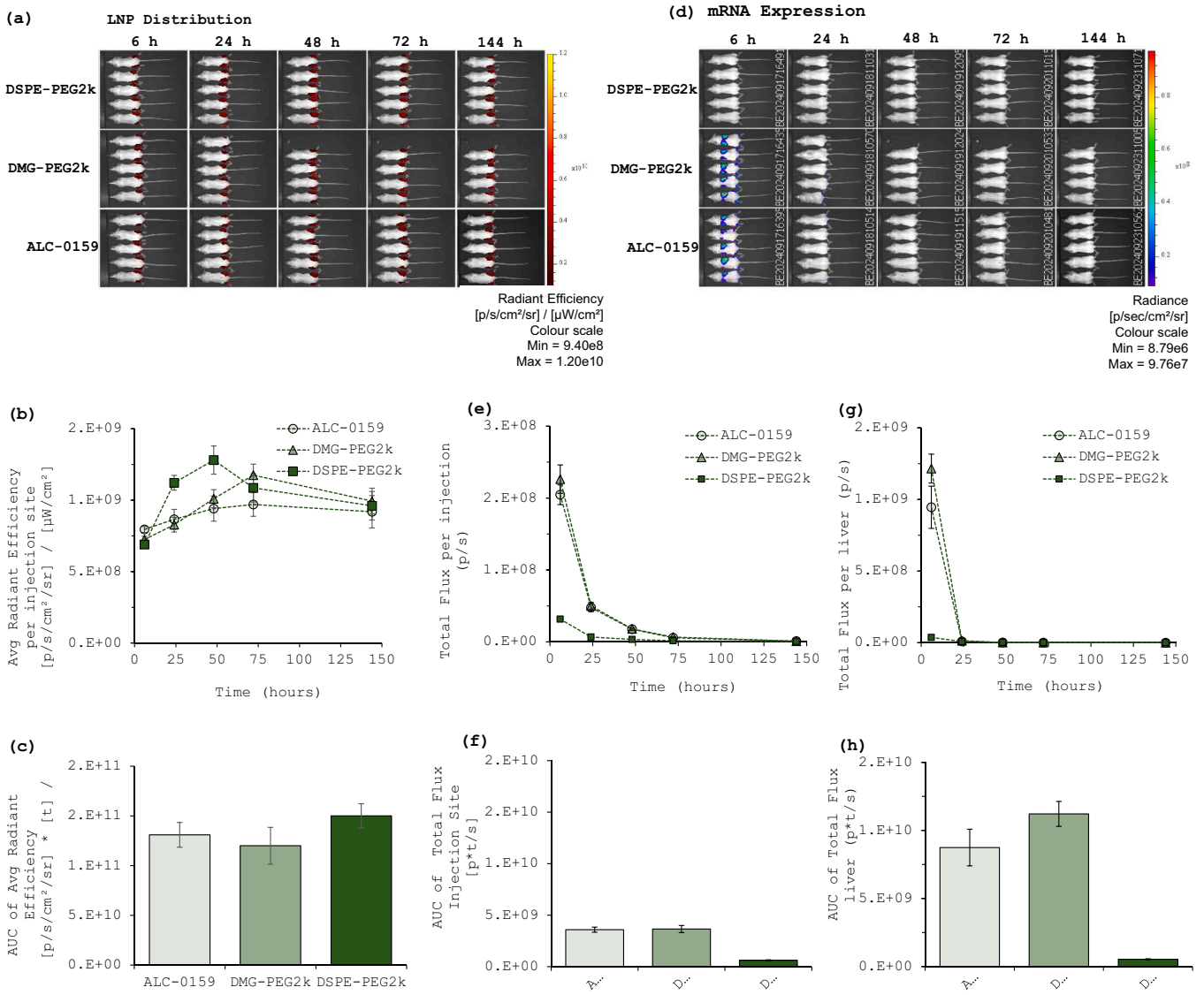

Fig. 8. Biodistribution and expression profile of MC3 Fluc mRNA-LNPs labelled with DiR prepared with three different PEGylated lipids (ALC-0159, DMG-PEG2k and DSPE-PEG2k), a) IVIS image representing the biodistribution profile of DiR labelled LNPs and b) the quantification of DIR intensity from the injection site over the time and c) the Area Under the Curve (AUC). d) Representative IVIS image of the expression profile of the LNPs formulated with Fluc mRNA and quantification of the luminescence signal as the light emitted from e) the injection site and g) corresponding Area Under the Curve (AUC) g) liver and corresponding h) the Area Under the Curve (AUC). The LNPs comprised DSPC: Chol: DLin-MC3-DMA (MC3): PEG lipid (10:38.5:50:1.5 M ratio) and encapsulated Fluc mRNA at NP6. PEG lipids are ALC-0159, DMG-PEG2k and DSPE-PEG2k. Female BALB/c mice were injected with 5 µg of Fluc mRNA-LNPs. Results represent mean ± SEM (5 mice, 1 injection per hind leg; 10 data points).

other hand, shorter C14 lipids tend to rapidly desorb, leading to their replacement by a protein corona. This protein corona significantly influences the subsequent destiny of the LNPs, resulting in a distinctly different outcome [39]. For example, Mui et al. examined the desorption rate of various PEGylated lipids having 3-different alkyl chains after IV injection. They showed PEG-lipid loss from LNPs *in vivo* to occur at >45%/hour, 1.3%/hour, and 0.2%/hour for C14, C16, and C18, respectively [20]. Thus, the steric barrier presented by C18 PEG-lipids could be considered permanent and confirms our finding, which shows DSPE-PEG reduces mRNA-LNP potency (Figs. 6–8). However, the interaction between the ionizable lipid and the PEG-lipid must also be considered. Indeed, it has been shown that PEG desorption rates may be linked to the choice of ionizable lipids, as SM-102 LNPs were shown to lose their PEG lipids more quickly compared to other ionizable lipids [39]. This underpins why the combination of lipids must be considered in the design of LNPs.

5. Conclusions

Overall, our studies confirm that for the development of mRNA LNP formulations, physico-chemical characteristics are indicative of the manufacturing process product quality but not potency indicating, and the prudent selection of *in vitro* and *in vivo* models is a pivotal factor in bridging the translation gap even within preclinical studies. *In vitro*, transfection efficiency exhibited a potency order of SM-102 > MC3 > DOTAP ≈ ALC-0315 > DODAP, whilst *in vivo* expression in BALB/c mice showed ALC-0315 LNPs displaying comparable potency to SM-102. While the choice of PEGylated lipid did not affect LNP clearance from the injection site, it significantly impacted potency. Specifically, longer-chain PEG lipids (C18) should be avoided, as they reduce efficacy. Moreover, there is a complex interaction between ionizable and PEGylated lipids, with the combination of ALC-0315 as the ionizable lipid and ALC-0159 as the PEGylated lipid yielding the highest protein expression.

Funding

This work was supported by the Ministry of National Education of the Republic of Türkiye (BB). YP acknowledges support from The Intracellular Drug Delivery Centre (IDDC) funded by UK Research and Innovation (UKRI). AZ acknowledges support from ERC-Stg Grant (MILKOSOMES No. 101115723). Views and opinions expressed are, however, those of the author(s) only and do not necessarily reflect those of the European Union or the European Research Council Executive Agency. Neither the European Union nor the granting authority can be held responsible for them.

Institutional Review Board Statement

All animals were handled in accordance with the UK Home Office Animals Scientific Procedures Act of 1986 in accordance with an internal ethics board and a UK government-approved project license (Project license PP1650440; Granted: 29 May 2020).

CRediT authorship contribution statement

Burcu Binici: Writing – review & editing, Writing – original draft, Visualization, Validation, Methodology, Investigation, Funding acquisition, Formal analysis, Data curation, Conceptualization. **Zahra Rattray:** Writing – review & editing, Writing – original draft, Visualization, Supervision, Methodology, Investigation, Formal analysis, Data curation, Conceptualization. **Assaf Zinger:** Writing – review & editing, Writing – original draft, Visualization, Methodology, Investigation, Formal analysis, Data curation, Conceptualization. **Yvonne Perrie:** Writing – review & editing, Writing – original draft, Validation, Supervision, Resources, Project administration, Methodology, Investigation, Funding acquisition, Formal analysis, Data curation, Conceptualization.

Declaration of competing interest

The authors declare that they have no known competing financial interests or personal relationships that could have appeared to influence the work reported in this paper.

Data availability

Data Availability Statement: The supporting dataset for this paper can be found at [https://doi.org/10.15129/a63f3a52-1753-46bf-9bf8-449bb4b9c16d].

Appendix A. Supplementary data

Supplementary data to this article can be found online at https://doi.org/10.1016/j.jconrel.2024.11.010.

References

[1] N. Pardi, M.J. Hogan, M.S. Naradikian, K. Parkhouse, D.W. Cain, L. Jones, M. A. Moody, H.P. Verkerke, A. Myles, E. Willis, C.C. LaBranche, D.C. Montefiori, J. L. Lobby, K.O. Saunders, H.-X. Liao, B.T. Korber, L.L. Sutherland, R.M. Scearce, P. T. Hraber, I. Tombácz, H. Muramatsu, H. Ni, D.A. Balikov, C. Li, B.L. Mui, Y. K. Tam, F. Krammer, K. Karikó, P. Polacino, L.C. Eisenlohr, T.D. Madden, M. J. Hope, M.G. Lewis, K.K. Lee, S.-L. Hu, S.E. Hensley, M.P. Cancro, B.F. Haynes, D. Weissman, Nucleoside-modified mRNA vaccines induce potent T follicular helper and germinal center B cell responses, J. Exp. Med. 215 (2018) 1571–1588, https://doi.org/10.1084/jem.20171450.

[2] M.D. Buschmann, M.J. Carrasco, S. Alishetty, M. Paige, M.G. Alameh, D. Weissman, Nanomaterial delivery systems for mrna vaccines, Vaccines (Basel) 9 (2021) 1–30, https://doi.org/10.3390/vaccines9010065.

[3] P. Sharma, D. Breier, D. Peer, Immunogenic amines on lipid nanoparticles, Nat. Biomed. Eng. (2024), https://doi.org/10.1038/s41551-024-01265-9.

[4] N. Chaudhary, L.N. Kasiewicz, A.N. Newby, M.L. Arral, S.S. Yerneni, J.R. Melamed, S.T. LoPresti, K.C. Fein, D.M. Strelkova Petersen, S. Kumar, R. Purwar, K. A. Whitehead, Amine headgroups in ionizable lipids drive immune responses to lipid nanoparticles by binding to the receptors TLR4 and CD1d, Nat, Biomed. Eng. (2024), https://doi.org/10.1038/s41551-024-01256-w.

[5] S. Ndeupen, Z. Qin, S. Jacobsen, A. Bouteau, H. Estanbouli, B.Z. Igyártó, The mRNA-LNP platform's lipid nanoparticle component used in preclinical vaccine studies is highly inflammatory, IScience 24 (2021) 103479, https://doi.org/10.1016/j.isci.2021.103479.

[6] J.A. Kulkarni, D. Witzigmann, J. Leung, Y.Y.C. Tam, P.R. Cullis, On the role of helper lipids in lipid nanoparticle formulations of siRNA, Nanoscale 11 (2019) 21733–21739, https://doi.org/10.1039/C9NR09347H.

[7] X. Cheng, R.J. Lee, The role of helper lipids in lipid nanoparticles (LNPs) designed for oligonucleotide delivery, Adv. Drug Deliv. Rev. 99 (2016) 129–137, https://doi.org/10.1016/j.addr.2016.01.022.

[8] C. Hald Albertsen, J.A. Kulkarni, D. Witzigmann, M. Lind, K. Petersson, J. B. Simonsen, The role of lipid components in lipid nanoparticles for vaccines and gene therapy, Adv. Drug Deliv. Rev. 188 (2022) 114416, https://doi.org/10.1016/j.addr.2022.114416.

[9] S. Patel, N. Ashwanikumar, E. Robinson, Y. Xia, C. Mihai, J.P. Griffith, S. Hou, A. A. Esposito, T. Ketova, K. Welsher, J.L. Joyal, Ö. Almarsson, G. Sahay, Naturally-occurring cholesterol analogues in lipid nanoparticles induce polymorphic shape and enhance intracellular delivery of mRNA, Nat. Commun. 11 (2020), https://doi.org/10.1038/s41467-020-14527-2.

[10] Y. Suzuki, H. Ishihara, Difference in the lipid nanoparticle technology employed in three approved siRNA (Patisiran) and mRNA (COVID-19 vaccine) drugs, Drug Metab. Pharmacokinet. 41 (2021) 100424, https://doi.org/10.1016/j.dmpk.2021.100424.

[11] S. Cui, Y. Wang, Y. Gong, X. Lin, Y. Zhao, D. Zhi, Q. Zhou, S. Zhang, Correlation of the cytotoxic effects of cationic lipids with their headgroups, Toxicol. Res. (Camb.) 7 (2018) 473–479, https://doi.org/10.1039/C8TX00005K.

[12] J.A. Kulkarni, P.R. Cullis, R. van der Meel, Lipid nanoparticles enabling gene therapies: from concepts to clinical utility, Nucleic Acid Ther. 28 (2018) 146–157, https://doi.org/10.1089/nat.2018.0721.

[13] K.J. Hassett, K.E. Benenato, E. Jacquinet, A. Lee, A. Woods, O. Yuzhakov, S. Himansu, J. Deterling, B.M. Geilich, T. Ketova, C. Mihai, A. Lynn, I. McFadyen, M.J. Moore, J.J. Senn, M.G. Stanton, Ö. Almarsson, G. Ciaramella, L.A. Brito, Optimization of lipid nanoparticles for intramuscular administration of mRNA vaccines, Mol. Ther. Nucleic Acids 15 (2019) 1–11, https://doi.org/10.1016/j.omtn.2019.01.013.

[14] E. Kon, U. Elia, D. Peer, Principles for designing an optimal mRNA lipid nanoparticle vaccine, Curr. Opin. Biotechnol. 73 (2022) 329–336, https://doi.org/10.1016/j.copbio.2021.09.016.

[15] F.P. Polack, S.J. Thomas, N. Kitchin, J. Absalon, A. Gurtman, S. Lockhart, J. L. Perez, G. Pérez Marc, E.D. Moreira, C. Zerbini, R. Bailey, K.A. Swanson, S. Roychoudhury, K. Koury, P. Li, W.V. Kalina, D. Cooper, R.W. Frenck, L. L. Hammitt, Ö. Türeci, H. Nell, A. Schaefer, S. Ünal, D.B. Tresnan, S. Mather, P. R. Dormitzer, U. Şahin, K.U. Jansen, W.C. Gruber, Safety and efficacy of the BNT162b2 mRNA Covid-19 vaccine, New Engl. J. Med. 383 (2020) 2603–2615, https://doi.org/10.1056/NEJMOA2034577/SUPPL_FILE/NEJMOA2034577_PROTOCOL.PDF.

[16] L.R. Baden, H.M. El Sahly, B. Essink, K. Kotloff, S. Frey, R. Novak, D. Diemert, S. A. Spector, N. Rouphael, C.B. Creech, J. McGettigan, S. Khetan, N. Segall, J. Solis, A. Brosz, C. Fierro, H. Schwartz, K. Neuzil, L. Corey, P. Gilbert, H. Janes, D. Follmann, M. Marovich, J. Mascola, L. Polakowski, J. Ledgerwood, B.S. Graham, H. Bennett, R. Pajon, C. Knightly, B. Leav, W. Deng, H. Zhou, S. Han, M. Ivarsson, J. Miller, T. Zaks, Efficacy and safety of the mRNA-1273 SARS-CoV-2 vaccine, N. Engl. J. Med. 384 (2021) 403–416, https://doi.org/10.1056/NEJMOA2035389/SUPPL_FILE/NEJMOA2035389_DATA-SHARING.PDF.

[17] A. Akinc, M.A. Maier, M. Manoharan, K. Fitzgerald, M. Jayaraman, S. Barros, S. Ansell, X. Du, M.J. Hope, T.D. Madden, B.L. Mui, S.C. Semple, Y.K. Tam, M. Ciufolini, D. Witzigmann, J.A. Kulkarni, R. van der Meel, P.R. Cullis, The Onpattro story and the clinical translation of nanomedicines containing nucleic acid-based drugs, Nat. Nanotechnol. 14 (2019) 1084–1087, https://doi.org/10.1038/s41565-019-0591-y.

[18] S. Li, Y. Hu, A. Li, J. Lin, K. Hsieh, Z. Schneiderman, P. Zhang, Y. Zhu, C. Qiu, E. Kokkoli, T.-H. Wang, H.-Q. Mao, Payload distribution and capacity of mRNA lipid nanoparticles, Nat. Commun. 13 (2022) 5561, https://doi.org/10.1038/s41467-022-33157-4.

[19] T. Suzuki, Y. Suzuki, T. Hihara, K. Kubara, K. Kondo, K. Hyodo, K. Yamazaki, T. Ishida, H. Ishihara, PEG shedding-rate-dependent blood clearance of PEGylated lipid nanoparticles in mice: faster PEG shedding attenuates anti-PEG IgM production, Int. J. Pharm. 588 (2020) 119792, https://doi.org/10.1016/j.ijpharm.2020.119792.

[20] B.L. Mui, Y.K. Tam, M. Jayaraman, S.M. Ansell, X. Du, Y.Y.C. Tam, P.J. Lin, S. Chen, J.K. Narayanannair, K.G. Rajeev, M. Manoharan, A. Akinc, M.A. Maier, P. Cullis, T.D. Madden, M.J. Hope, Influence of polyethylene glycol lipid desorption rates on pharmacokinetics and pharmacodynamics of siRNA lipid nanoparticles, Mol. Ther. Nucleic Acids 2 (2013) e139, https://doi.org/10.1038/mtna.2013.66.

[21] M.J. Carrasco, S. Alishetty, M.-G. Alameh, H. Said, L. Wright, M. Paige, O. Soliman, D. Weissman, T.E. Cleveland, A. Grishaev, M.D. Buschmann, Ionization and structural properties of mRNA lipid nanoparticles influence expression in intramuscular and intravascular administration, Commun. Biol. 4 (2021) 956, https://doi.org/10.1038/s42003-021-02441-2.

[22] S. Anthiya, S.C. Öztürk, H. Yanik, E. Tavukcuoglu, A. Şahin, D. Datta, K. Charisse, D.M. Álvarez, M.I. Loza, A. Calvo, E. Sulheim, S. Loevenich, G. Klinkenberg, R. Schmid, M. Manoharan, G. Esendağlı, M.J. Alonso, Targeted siRNA lipid

nanoparticles for the treatment of KRAS-mutant tumors, J. Control. Release 357 (2023) 67–83, https://doi.org/10.1016/j.jconrel.2023.03.016.
[23] R.J. Mow, A. Srinivasan, E. Bolay, D. Merlin, C. Yang, Fluorescent labeling and imaging of IL-22 mRNA-loaded lipid nanoparticles, Bio-Protoc. 14 (2024), https://doi.org/10.21769/BioProtoc.4994.
[24] R. Ma, Y. Li, Y. Wei, J. Zhou, J. Ma, M. Zhang, J. Tu, J. Jiang, S. Xie, W. Tan, X. Liu, The dynamic process of mRNA delivery by lipid nanoparticles in vivo, Nano Today 57 (2024) 102325, https://doi.org/10.1016/J.NANTOD.2024.102325.
[25] J. Di, Z. Du, K. Wu, S. Jin, X. Wang, T. Li, Y. Xu, Biodistribution and non-linear gene expression of mRNA LNPs affected by delivery route and particle size, Pharm. Res. 39 (2022) 105–114, https://doi.org/10.1007/s11095-022-03166-5.
[26] C. McMillan, A. Druschitz, S. Rumbelow, A. Borah, B. Binici, Z. Rattray, Y. Perrie, Tailoring lipid nanoparticle dimensions through manufacturing processes, RSC Pharmaceut. 1 (2024) 841–853, https://doi.org/10.1039/D4PM00128A.
[27] O. Escalona-Rayo, Y. Zeng, R.A. Knol, T.J.F. Kock, D. Aschmann, B. Slütter, A. Kros, In vitro and in vivo evaluation of clinically-approved ionizable cationic lipids shows divergent results between mRNA transfection and vaccine efficacy, Biomed. Pharmacother. 165 (2023) 115065, https://doi.org/10.1016/j.biopha.2023.115065.
[28] W. Zhang, A. Pfeifle, C. Lansdell, G. Frahm, J. Cecillon, L. Tamming, C. Gravel, J. Gao, S.N. Thulasi Raman, L. Wang, S. Sauve, M. Rosu-Myles, X. Li, M.J. W. Johnston, The expression kinetics and immunogenicity of lipid nanoparticles delivering plasmid DNA and mRNA in mice, Vaccines (Basel) 11 (2023) 1580, https://doi.org/10.3390/vaccines11101580.
[29] G. Tilstra, J. Couture-Senécal, Y.M.A. Lau, A.M. Manning, D.S.M. Wong, W. W. Janaeska, T.A. Wuraola, J. Pang, O.F. Khan, Iterative design of ionizable lipids for intramuscular mRNA delivery, J. Am. Chem. Soc. 145 (2023) 2294–2304, https://doi.org/10.1021/jacs.2c10670.
[30] K. Hashiba, Y. Sato, M. Taguchi, S. Sakamoto, A. Otsu, Y. Maeda, T. Shishido, M. Murakawa, A. Okazaki, H. Harashima, Branching ionizable lipids can enhance the stability, fusogenicity, and functional delivery of mRNA, Small Sci. 3 (2023), https://doi.org/10.1002/smsc.202200071.
[31] K.A. Hajj, R.L. Ball, S.B. Deluty, S.R. Singh, D. Strelkova, C.M. Knapp, K. A. Whitehead, Branched-tail lipid nanoparticles potently deliver mRNA in vivo due to enhanced ionization at endosomal pH, Small 15 (2019), https://doi.org/10.1002/smll.201805097.
[32] Y. Zhang, C. Sun, C. Wang, K.E. Jankovic, Y. Dong, Lipids and lipid derivatives for RNA delivery, Chem. Rev. 121 (2021) 12181–12277, https://doi.org/10.1021/acs.chemrev.1c00244.
[33] Y. Sato, K. Hashiba, K. Sasaki, M. Maeki, M. Tokeshi, H. Harashima, Understanding structure-activity relationships of pH-sensitive cationic lipids facilitates the rational identification of promising lipid nanoparticles for delivering siRNAs in vivo, J. Control. Release 295 (2019) 140–152, https://doi.org/10.1016/j.jconrel.2019.01.001.
[34] C. Mancino, J. Pollet, A. Zinger, K.M. Jones, M.J. Villar, A.C. Leao, R. Adhikari, L. Versteeg, R. Tyagi Kundu, U. Strych, F. Giordano, P.J. Hotez, M.E. Bottazzi, F. Taraballi, C. Poveda, Harnessing RNA technology to advance therapeutic vaccine antigens against Chagas disease, ACS Appl. Mater. Interfaces 16 (2024) 15832–15846, https://doi.org/10.1021/acsami.3c18830.
[35] F. Ferraresso, A.W. Strilchuk, L.J. Juang, L.G. Poole, J.P. Luyendyk, C.J. Kastrup, Comparison of DLin-MC3-DMA and ALC-0315 for siRNA delivery to hepatocytes and hepatic stellate cells, Mol. Pharm. 19 (2022) 2175–2182, https://doi.org/10.1021/acs.molpharmaceut.2c00033.
[36] S. Sabnis, E.S. Kumarasinghe, T. Salerno, C. Mihai, T. Ketova, J.J. Senn, A. Lynn, A. Bulychev, I. McFadyen, J. Chan, Ö. Almarsson, M.G. Stanton, K.E. Benenato, A novel amino lipid series for mRNA delivery: improved endosomal escape and sustained pharmacology and safety in non-human primates, Mol. Ther. 26 (2018) 1509–1519, https://doi.org/10.1016/J.YMTHE.2018.03.010.
[37] S. Ramishetti, I. Hazan-Halevy, R. Palakuri, S. Chatterjee, S. Naidu Gonna, N. Dammes, I. Freilich, L. Kolik Shmuel, D. Danino, D. Peer, A combinatorial library of lipid nanoparticles for RNA delivery to leukocytes, Adv. Mater. 32 (2020), https://doi.org/10.1002/adma.201906128.
[38] G.S. Naidu, S.-B. Yong, S. Ramishetti, R. Rampado, P. Sharma, A. Ezra, M. Goldsmith, I. Hazan-Halevy, S. Chatterjee, A. Aitha, D. Peer, A combinatorial library of lipid nanoparticles for cell type-specific mRNA delivery, Adv. Sci. (Weinh.) 10 (2023) e2301929, https://doi.org/10.1002/advs.202301929.
[39] M. Berger, M. Degey, J. Leblond Chain, E. Maquoi, B. Evrard, A. Lechanteur, G. Piel, Effect of PEG anchor and serum on lipid nanoparticles: development of a nanoparticles tracking method, Pharmaceutics 15 (2023) 597, https://doi.org/10.3390/pharmaceutics15020597.